Science and Technology Indonesia
e-ISSN:2580-4391 p-ISSN:2580-4405
Vol. 8, No. 4, October 2023

Research Paper

Green Synthesis of KO Nanoparticles by Cold Plasma and Study of Their Properties for Antibacterial Applications

Mohammed Jawad Kadhim[1], Rana Ismael Khaleel[1], Karar Mahdi Talib[2], Raghad S. Mohammed[1]*

[1]*Department of Physics, College of Science, Mustansiriyah University, Baghdad, 14022, Iraq*
[2]*Department of Basic Science, College of Dentistry, Al-Muthanna University, Samawa, 66001, Iraq*
***Corresponding author**: raghad.almaliki@uomustansiriyah.edu.iq

Abstract
This study used the cold plasma technique to synthesize potassium oxide nanoparticles (KO NPs) from potassium chloride (KCl) with roselle extract leaves and examine their physical and biological characterization. The physical properties of KO nanoparticles were examined by Scanning Electron Microscopy (SEM), X-Ray Diffraction (XRD), X-Ray Dispersive Spectroscopy (EDS), and UV–Vis Spectroscopy. Analyses of XRD show the KO NPs with an average crystallite size of 108 nm. The EDX analysis shows that high-purity KO NPs have formed. SEM image shows the shapes of some KO NPs' spherical with varying sizes ranging from 44.66 nm to 134 nm. According to UV–Vis spectra of KO NPs, the absorption edge of these nanoparticles exhibited a blueshift with an energy gap range (E_g) from 2.8 to 3.4 eV. The biological efficacy of KO NPs was also examined by testing their antibacterial and antifungal activity. To evaluate the toxicity of the KO NPs were tested in vitro and activated as antibacterial. Against some of the test organisms, the KO NPs demonstrated good antibacterial activity.

Keywords
KO Nanoparticles, Green Synthesis, Structural Properties, Optical Properties, Plasma Jets, Cold Plasma

Received: 11 May 2023, Accepted: 20 July 2023
https://doi.org/10.26554/sti.2023.8.4.579-584

1. INTRODUCTION

Nanomaterials have garnered considerable interest due to their distinct properties in comparison to their bulk counterparts. Due to their unique chemical and physical properties, small sizes, and large surface areas, nanoparticles are applicable to a wide spectrum of applications (Jin and Jin, 2019; Mohammed et al., 2022b). Various scientific societies, spanning from medicine to engineering, are conducting extensive research and producing novel materials to meet their specific needs. The most pressing requirement in the biomedical field is the development of biocompatible nanomaterials, as biocompatibility is a critical criterion that must be established before practical applications can be considered (Khanna and Verma, 2014). New opportunities for biological applications are made possible by nanotechnology by changing the physicochemical properties of substances Mohammed et al. (2022b). This is significant since many different NPs, including those that are resistant to antibiotics, have been found to be effective against a wide variety of diseases in recent years.

The effectiveness of nanoparticles against microorganisms is affected by a variety of parameters, including their size, surface area, shape, net charge, and physicochemical properties (Ozdal and Gurkok, 2022; Mohammed et al., 2023). Using physical and chemical methods, nanoparticles of different materials have been created. Different techniques, such as pulsed laser deposition, thermal decomposition, hydrothermal procedures, sol-gel preparation, chemical coprecipitation, etc., may be used to create nanoparticles (Mohammed et al., 2022a; Abbasalipourkabir et al., 2015). Traditional methods have been used for years to generate NPs, but research has shown that green approaches are more effective and cheaper, with fewer failures and easier characterization. In a few minutes to a few hours at room temperature, a metal salt is produced with plant extract (Hussain et al., 2016; Gour and Jain, 2019).

Non-thermal plasmas, also called "cold plasma" have recently received great attention for their beneficial properties and many industrial applications, such as processing materials, electronics, and polymers. In the last few years, the number of biomedical devices and biological materials that can be used with cold plasma has grown quickly (Yatom et al., 2017). Cold plasma synthesis of nanoparticles is a good alternative to chemical synthesis that proves efficient and eco-friendly alternative (Nguyen et al., 2021). This technique has succeeded in the synthesis of many nanoparticles. Many experimental investi-

gations have been carried out to synthesize nanoparticles by plasma technique, synthesize two hybrid classes of NPs by argon plasma jets, these NPs were MgO/ZnO and CuO/ZnO core/shell NPs and study of their physical characterization and application in vivo to determine its beneficial medical applications (Mohammed et al., 2022b; Mohammed et al., 2022a; Mohammed et al., 2023). Also, Shuaib et al. (2020) synthesis of Ag NPs by microplasma technique and exam of their antibacterial and antifungal applications. In a recent study by Kaushik et al. (2023), nitric oxide-enriched plasma-activated water turned off and changed the antiviral response genes of the 229E coronavirus in human lung host cells.

This study aimed to synthesize KO nanoparticles with roselle extract leaves by cold argon plasma-activated potassium chloride solution and study their physical properties and exam of their bioactivated in vitro as antibacterial. The reason for choosing the Roselle plant in our study is several studies have demonstrated that Roselle plants are a good source of natural antioxidants (Carvajal-Zarrabal et al., 2009). Moreover, roselle extracts have antimicrobial activity against a variety of pathogenic microorganisms (Morales-Cabrera et al., 2013; Kamali and Mohammed, 2006; Fullerton et al., 2011).

2. EXPERIMENTAL SECTION

2.1 Material and Methods

Potassium chloride (KCl) with purity (99.99%) was used to synthesize KO nanoparticles. The roselle extract leaves were collected from the local market in Baghdad.

2.2 Preparation of Roselle Extract Leaves

The roselle extract leaves have been cleaned with deionized water to remove dirt and debris, dried, and then ground in preparation for use. Take 50 g of it, add 500 mL of deionized water, bolling, and filter with filter paper. The green synthesis of KO NPs included the use of roselle extract as a reducing and capping agent.

2.3 Setup of the Cold Plasma Device

The experimental configuration of the plasma jet system utilized to produce KO NPs is shown in Figure 1. The plasma jet device consisted of an AC high-voltage (8 kV) and two stainless steel electrodes. The first electrode, designed as a hollow needle, acted as the cathode for gas to pass through, and the other electrode was immersed in a glass beaker containing Potassium chloride solution and roselle extract leaves. The gas discharge was argon gas with 99.99% purity, and the gas rate, measured by a flowmeter, was 2 (L/min).

2.4 Synthesize KO NPs from Roselle Extract Leaves by Cold Plasma Device

Three concentrations (0.4 M, 0.8 M, and 1.6 M) of KCl have been prepared by dissolving potassium chloride (KCl) in 20 mL of deionized water and placing the solution on a magnetic stirrer at 80°C for 15 min until it is completely dissolved. After adding 3 mL of the extract with 7 mL of the solution of KO, and the plasma exposure time of 3 min. The physical characterization of the synthesized KO nanoparticles was examined by XRD, SEM, EDS, and UV-Vis. The biological efficacy of KO NPs was also examined by testing their antibacterial and antifungal activity.

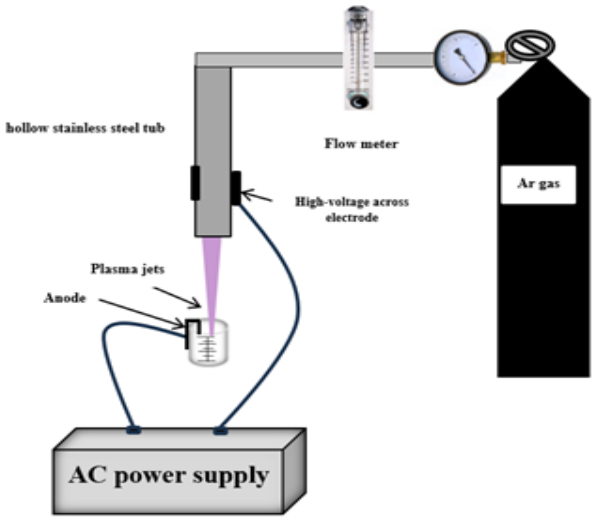

Figure 1. The Experimental Configuration for the Cold Plasma Device used to Create KO NPs

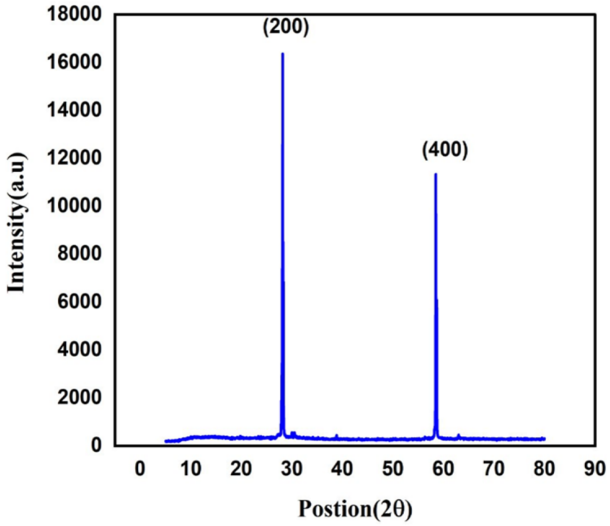

Figure 2. XRD Pattern of KO NPs Synthesis by Cold Plasma

2.5 Antibacterial Test

Type of bacteria (*Staphylococcus*, *S. epidermidis*, *Klebsiella spp.*, *Escherichia coli*, *Candida albicans*, *Salmonella*) were obtained from the Department of Biology, College of Science, Mustansiriayah University, to examine the antimicrobial properties of KO NPs synthesized by cold plasma. To estimate the antimicrobial activity of KO NPs the agar well diffusion method has been used.

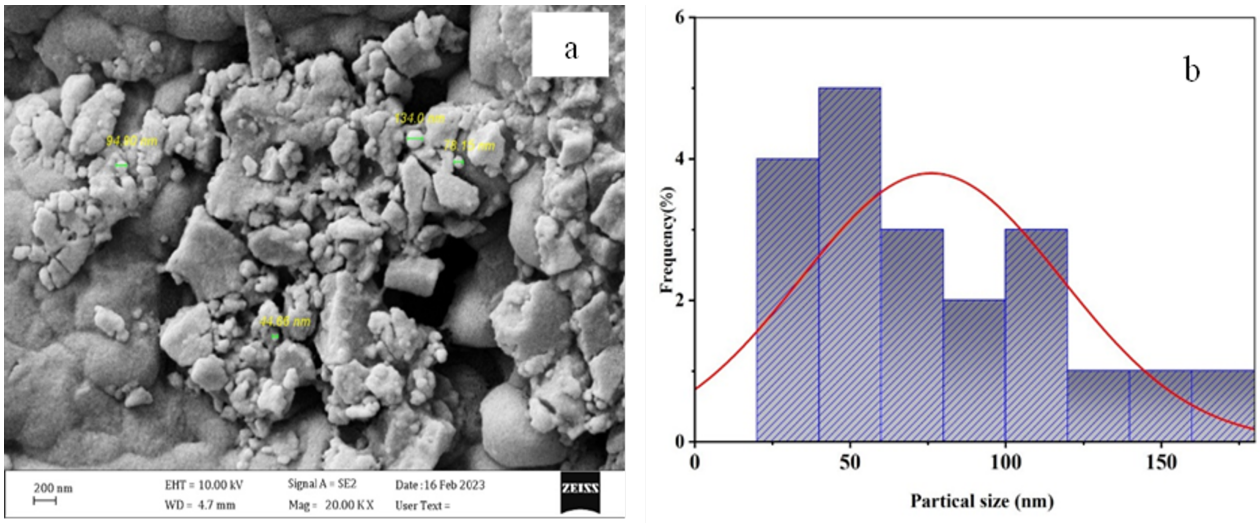

Figure 3. (a): SEM Images of KO NPs Synthesized by Cold Plasma. (b): Histogram of Distribution Particle Size

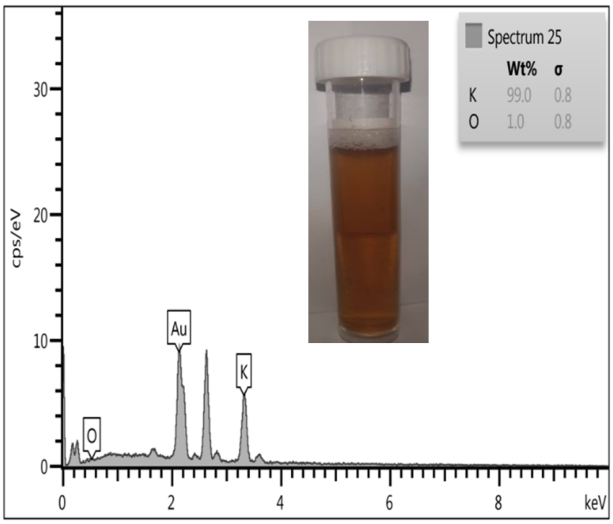

Figure 4. EDX Spectra of the KO NPs Synthesized by Cold Plasma

3. RESULTS AND DISCUSSION

3.1 XRD Analyses

The crystal structure and phase purity of the KO NPs synthesized through the cold plasma (CP) technique were verified via X-ray Diffraction (XRD) analysis by comparing the KO diffraction angle (2θ) with the literature JCPDS card No. Figure 2 shows that the XRD pattern was taken at an angle of $2\theta^{\circ}$ ranging from 25° to 70°. The KO structure is associated with diffraction peaks in the XRD pattern of KO NPs at 28.26° and 58.48°, which are indexed to miller indices (200) and (400), respectively. Having been matched with the KO cube structure (JCPDS No: 41-1476). Using the Scherrer Equation, the crystallite size of KO NPs was determined (Ali et al., 2017):

$$D(\text{Å}) = \frac{k\lambda}{\beta \cos\theta} \quad (1)$$

Here: D: is the average crystallite size, λ is the X-rays wavelength (1.540 Å), k: is constant (k = 0.9), and β is defined as the full width at half maximum (FWHM) of the peaks diffraction. The average crystalline size of KO nanoparticles was 108 nm.

3.2 Analyses of SEM and EDX

The form of KO nanoparticles produced by the cold plasma method was studied using Scanning Electron Microscopy (SEM) images. The images obtained from an SEM show that the particles made have the shape and size of nanoparticles. The large size grains can be noticed in Figure 3a, and the NPs' aggregation may have something to do with the extra surface area. Attractive physical forces between the nanoparticles were maintained by their larger surface area to volume ratio, keeping them agglomerated (Hong et al., 2006; Mohammed et al., 2022b). According to the SEM image, Figure 3a shows the spherical shapes of some KO NPs with varying sizes ranging from 44.66 nm to 134 nm, the histogram of the distribution of KO particle size, as shown in Figure 3b.

The KO NPs' specific chemical structure was analyzed using Energy Dispersive X-Ray (EDX) technique. As shown in Figure 4, the EDX spectrum shows that there are peaks for the elements K and O. EDX analysis verified that there were no additional elements present in the KO NPs composition, this confirms the purity of synthesized KO NPs by cold plasma method. The K and O percentage compositions of KO NPs were listed in shown in Figure 4.

3.3 Optical Properties

Light absorption by the sample is the basis of the UV/ Vis spectrophotometer. The optical parameter of most importance is

the bandgap. The UV-Vis absorption spectra of KO nanoparticles were displayed in Figure 5 as a function of wavelength. From 200 to 450 nm in wavelength range, a large absorption peak is observed. Figure 5 shows the optical absorption of KO NPs. We found an indication of a redshift in the absorption edge of these nanoparticles. Due to their redshift behavior, KO NPs are predicted to have a smaller optical band gap (E_g). Kumar et al. (2013) hypothesized that the redshift may have been caused by aggregation in the nanoparticles.

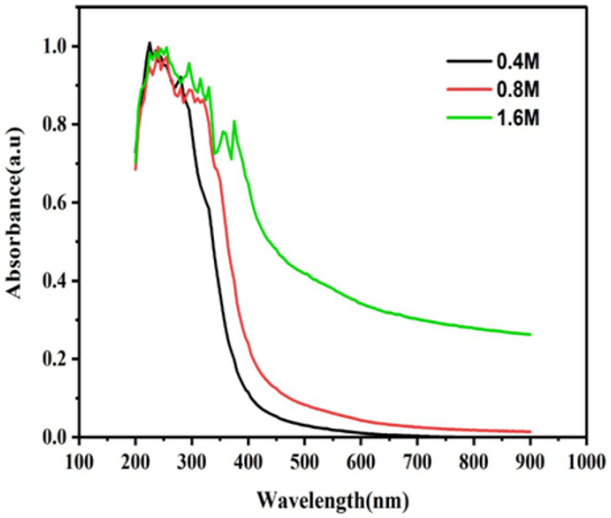

Figure 5. Optical Absorption Spectra of KO NPs

From absorbance spectra and using Tauc's relation Equation 2 (Pradeev Raj et al., 2018) for direct transition, the absorption coefficient of KO NPs was calculated graphically.

$$(\alpha h\nu)^r = A(h\nu - E_g) \quad (2)$$

In this equation, r is a variable that depends on the kind of transition being permitted (r = 2 for allowed direct transition), A is a constant (0.9), E_g is the optical energy gap, α is the absorption coefficient, ν is the frequency of the photon, and, h: is plank's constant. As shown in Figure 6, bandgaps are often determined by creating a graph between photon energy hν) and $(\alpha h\nu)^r$ and then projecting the straight line to the axis intercept. For the KO NPs, the bandgap energies were 2.8 eV, 3.25 eV, and 3.4 eV for 0.4 M, 0.8 M, and 1.6 M concentrations, respectively. These findings differed from those published in the literature review, where it was less than the energy gap value published in the previous literature Constantino-Alcazar et al. (2021).

3.4 KO NPs' Antibacterial Effects

The KO NPs showed antibacterial action against a particular group of test organisms. Table 1 appears the value of the inhibition zone of varied concentrations of KO NPs (0.4, 0.8, and 1.6 M) synthesis by the plasma jets method. The diameter of the inhibition zone (DIZ) was measured using the well disc diffusion

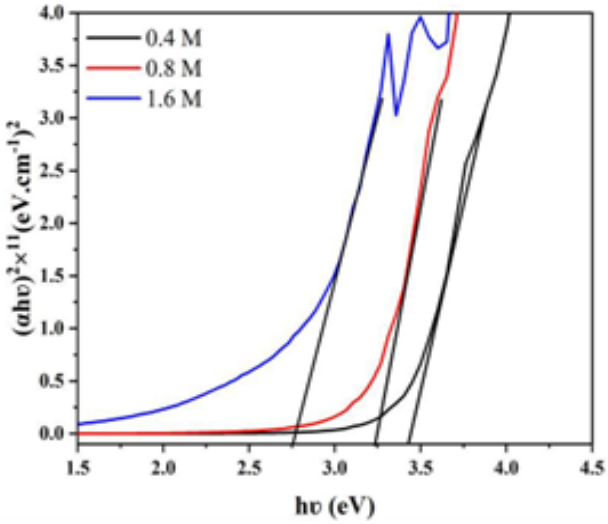

Figure 6. The Optical Band Gap for KO NPs

technique for 6 different bacterial and fungal species, including two Gram-positive (*Staphylococcus aureus*, *Staphylococcus epidermis*) and three Gram-negative (*Escherichia coli*, *Klebsiella spp*, *Salm*, *Salmonella*), and (*Candida albicans*). It was noticed that the good activity for the highest concentration of KO NPs (1.6 M) against *E. coli* with a zone of inhibition of 14 mm, and for the lowest concentration (0.4 M) the DIZ was 9 mm. While it was a less determined zone of growth inhibition towards *Salmonella* treated with KO NPs for the highest concentration (1.6 M) the DIZ was 11 mm, and for the lowest concentration (0.4 M) the DIZ was 6 mm. The outcomes of the inhibition zone of our study are less than those reported in previous studies, a study conducted by Ismail et al. (2022) reported good activity of PO NPs prepared from KCl with *Curcuma longa* plant against *S. epidermidis* bacteria where was the inhibition rate 31 nm. While Raj et al. (2016) demonstrated that PZ NPs had significant antibacterial action against *P. aernginosa*, with an approximately 20 mm zone of inhibition. The interaction, particle size, shape, and response between biomolecules and nanoparticles, as well as the presence of reactive oxygen species (ROS), are all crucial factors in determining whether or not nanoparticles will be effective against bacteria. The toxic effects of dissolving the outer membrane of the bacterium may be responsible for the inhibition (Yu et al., 2012). This is because oxidative stress created by reactive oxygen species (ROS) from metal/oxide nanoparticles causes the membrane to rupture. The production of reactive oxygen species (ROS) is a key NPs toxicity mechanism for bacterial cells. Interactions between cells and NPs damage mitochondria, microfilaments, or nuclei. Indirect interactions cause ROS to be released either inside or outside of the cell. Cellular absorption and the generation of ROS are two potential methods by which NPs interact with bacterial cells (Joo and Aggarwal, 2018). To demonstrate their efficacy in the field against pathogen microorganisms, further study of the nanotoxicity of KO NPs at varying concentrations is necessary.

Figure 7 show the inhibition zone of varied concentration of KO NPs.

Table 1. The Inhibition Zone of Varied Concentrations of KO NPs

Bactria Type	Inhibition Zone (mm)		
	0.4 M	0.8 M	1.6 M
Staphyloccus aureus	10	10	-
Staphyloccus epidermidis	10	10	-
Escherichia coli	9	-	14
Klebsiella sp.	9	9	12
Candida albicans	-	-	-
Salmonella	6	10	11

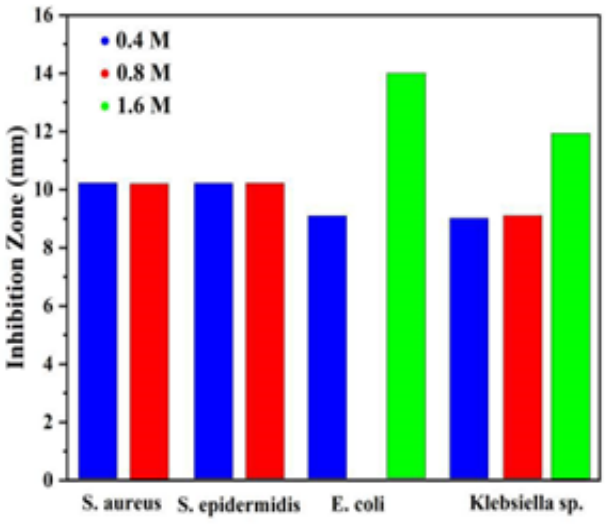

Figure 7. Comparing the Antibacterial Efficacy of KO NPs

4. CONCLUSION

The cold plasma technique has successfully synthesized the KO NPs with roselle extract leaves. This synthesis technique provides nanoparticles with high purity according to XRD and EDX analysis. XRD results show that the average crystallite size was 108 nm. SEM results exhibit the formation of aggregated small particles. The results obtained from our study demonstrate that the KO NPs exhibited antibacterial activity at 1.6 M concentration. To demonstrate the KO NPs' efficacy in combating pathogen microorganisms, more nanotoxicity studies of KO NPs at varying dosages are necessary.

5. ACKNOWLEDGMENT

This study is supported by the Department of Biology, College of Science, Mustansiriayah University.

REFERENCES

Abbasalipourkabir, R., H. Moradi, S. Zarei, S. Asadi, A. Salehzadeh, A. Ghafourikhosroshahi, M. Mortazavi, and N. Ziamajidi (2015). Toxicity of Zinc Oxide Nanoparticles on Adult Male Wistar Rats. *Food and Chemical Toxicology*, **84**; 154–160

Ali, A., Y. Rammah, R. El-Mallawany, and D. Souri (2017). FTIR and UV Spectra of Pentaternary Borate Glasses. *Measurement*, **105**; 72–77

Carvajal-Zarrabal, O., P. Hayward-Jones, Z. Orta-Flores, C. Nolasco-Hipólito, D. Barradas-Dermitz, M. Aguilar-Uscanga, and M. Pedroza-Hernández (2009). Effect of *Hibiscus sabdariffa L.* Dried Calyx Ethanol Extract on Fat Absorption-Excretion, and Body Weight Implication in Rats. *BioMed Research International*, **2009**; 394592

Constantino-Alcazar, J., M. Abud-Archila, B. Valdez-Salas, F. Gutierrez-Miceli, C. Ceceña-Duran, B. López-Valenzuela, and D. Gonzalez-Mendoza (2021). Synthesis and Characterization of Green Potassium Nanoparticles from Sideroxylon Capiri and Evaluation of Their Potential Antimicrobial. *Journal of Renewable Materials*, **9**(10); 1699–1706

Fullerton, M., J. Khatiwada, J. U. Johnson, S. Davis, and L. L. Williams (2011). Determination of Antimicrobial Activity of Sorrel (*Hibiscus sabdariffa*) on *Escherichia coli* O157: H7 Isolated from Food, Veterinary, and Clinical Samples. *Journal of Medicinal Food*, **14**(9); 950–956

Gour, A. and N. K. Jain (2019). Advances in Green Synthesis of Nanoparticles. *Artificial Cells, Nanomedicine, and Biotechnology*, **47**(1); 844–851

Hong, R., J. Qian, and J. Cao (2006). Synthesis and Characterization of PMMA Grafted ZnO Nanoparticles. *Powder Technology*, **163**(3); 160–168

Hussain, I., N. Singh, A. Singh, H. Singh, and S. Singh (2016). Green Synthesis of Nanoparticles and its Potential Application. *Biotechnology Letters*, **38**; 545–560

Ismail, S. N., E. m. Ali, B. J. Alwan, and A. N. Abd (2022). Potassium Chloride Nanoparticles: Synthesis, Characterization, and Study the Antimicrobial Applications. *Macromolecular Symposia*, **401**(1); 2100312

Jin, S. E. and H. E. Jin (2019). Synthesis, Characterization, and Three-Dimensional Structure Generation of Zinc Oxide-Based Nanomedicine for Biomedical Applications. *Pharmaceutics*, **11**(11); 575

Joo, S. H. and S. Aggarwal (2018). Factors Impacting the Interactions of Engineered Nanoparticles with Bacterial Cells and Biofilms: Mechanistic Insights and State of Knowledge. *Journal of Environmental Management*, **225**; 62–74

Kamali, H. and M. F. Mohammed (2006). Antibacterial Activity of *Hibiscus sabdariffa*, *Acacia seyal var. seyal* and *Sphaeranthus suaveolens var. suaveolens* Against Upper Respiratory Tract Pathogens. *Sudan Journal of Medical Sciences*, **1**(2); 121–126

Kaushik, N. K., P. Bhartiya, N. Kaushik, Y. Shin, L. N. Nguyen, J. S. Park, D. Kim, and E. H. Choi (2023). Nitric-Oxide

Enriched Plasma-Activated Water Inactivates 229E Coronavirus and Alters Antiviral Response Genes in Human Lung Host Cells. *Bioactive Materials*, **19**; 569–580

Khanna, L. and N. Verma (2014). Synthesis, Characterization and Biocompatibility of Potassium Ferrite Nanoparticles. *Journal of Materials Science & Technology*, **30**(1); 30–36

Kumar, S. S., P. Venkateswarlu, V. R. Rao, and G. N. Rao (2013). Synthesis, Characterization and Optical Properties of Zinc Oxide Nanoparticles. *International Nano Letters*, **3**; 1–6

Mohammed, R. S., K. A. Aadim, and K. A. Ahmed (2022a). Estimation of in Vivo Toxicity of MgO/ZnO Core/Shell Nanoparticles Synthesized by Eco-Friendly Non-Thermal Plasma Technology. *Applied Nanoscience*, **12**(12); 3783–3795

Mohammed, R. S., K. A. Aadim, and K. A. Ahmed (2022b). Synthesis of CuO/ZnO and MgO/ZnO Core/Shell Nanoparticles with Plasma Jets and Study of Their Structural and Optical Properties. *Karbala International Journal of Modern Science*, **8**(2); 88–97

Mohammed, R. S., K. A. Aadim, and K. A. Ahmed (2023). Histological, Haematological, and Thyroid Hormones Toxicity of Female Rats Orally Exposed to CuO/ZnO Core/Shell Nanoparticles Synthesized by Ar Plasma Jets. *Archives of Toxicology*, **97**(4); 1017–1031

Morales-Cabrera, M., J. Hernández-Morales, G. Leyva-Rúelas, Y. Salinas-Moreno, L. Soto-Rojas, and J. Castro-Rosas (2013). Influence of Variety and Extraction Solvent on Antibacterial Activity of Roselle (*Hibiscus sabdariffa L.*) Calyxes. *Journal of Medicinal Plants Research*, **7**(31); 2319–2322

Nguyen, L. N., P. Lamichhane, E. H. Choi, and G. J. Lee (2021). Structural and Optical Sensing Properties of Nonthermal Atmospheric Plasma-Synthesized Polyethylene Glycol-Functionalized Gold Nanoparticles. *Nanomaterials*, **11**(7); 1678

Ozdal, M. and S. Gurkok (2022). Recent Advances in Nanoparticles as Antibacterial Agent. *ADMET and DMPK*, **10**(2); 115–129

Pradeev Raj, K., K. Sadaiyandi, A. Kennedy, S. Sagadevan, Z. Z. Chowdhury, M. R. B. Johan, F. A. Aziz, R. F. Rafique, R. Thamiz Selvi, and R. Rathina Bala (2018). Influence of Mg Doping on ZnO Nanoparticles for Enhanced Photocatalytic Evaluation and Antibacterial Analysis. *Nanoscale Research Letters*, **13**; 1–13

Raj, R. B., M. Umadevi, V. P. Parvathi, and R. Parimaladevi (2016). Effect of Potassium on Structural, Photocatalytic and Antibacterial Activities of ZnO Nanoparticles. *Advances in Natural Sciences: Nanoscience and Nanotechnology*, **7**(4); 045008

Shuaib, U., T. Hussain, R. Ahmad, M. Zakaullah, F. E. Mubarik, S. T. Muntaha, and S. Ashraf (2020). Plasma-Liquid Synthesis of Silver Nanoparticles and Their Antibacterial and Antifungal Applications. *Materials Research Express*, **7**(3); 035015

Yatom, S., Y. Luo, Q. Xiong, and P. J. Bruggeman (2017). Nanosecond Pulsed Humid Ar Plasma Jet in Air: Shielding, Discharge Characteristics and Atomic Hydrogen Production. *Journal of Physics D: Applied Physics*, **50**(41); 415204

Yu, B., Y. Zhang, W. Zheng, C. Fan, and T. Chen (2012). Positive Surface Charge Enhances Selective Cellular Uptake and Anticancer Efficacy of Selenium Nanoparticles. *Inorganic Chemistry*, **51**(16); 8956–8963

